

Unification Model of Active Galactic Nuclei by Photoionization Equilibrium Calculation Based on Radiative Hydrodynamic Simulations

ATSUSHI TANIMOTO ¹, KEIICHI WADA ^{1, 2, 3}, YUKI KUDO ⁴, NOZOMU KAWAKATU ⁵, MARIKO NOMURA ⁶ AND
 HIROKAZU ODAKA ⁷

¹*Graduate School of Science and Engineering, Kagoshima University, Kagoshima 890-0065, Japan*

²*Research Center for Space and Cosmic Evolution, Ehime University, Matsuyama 790-8577, Japan*

³*Faculty of Science, Hokkaido University, Sapporo 060-0810, Japan*

⁴*Astronomical Institute, Tohoku University, Miyagi 980-8578, Japan*

⁵*Faculty of Natural Sciences, National Institute of Technology, Kure College, Hiroshima 737-8506, Japan*

⁶*Graduate School of Science and Technology, Hirosaki University, Aomori, 036-8561, Japan*

⁷*Department of Earth and Space Science, The University of Osaka, Osaka 560-0043, Japan*

ABSTRACT

To investigate the origin of the dependence of the covering factor on the Eddington ratio suggested by X-ray observations, we examined the angular distribution of H I and H II based on two-dimensional radiative hydrodynamic simulations. To calculate the Compton-thin covering factor C_{22} and Compton-thick covering factor C_{24} of H I alone, we performed one-dimensional photoionization equilibrium calculations with the XSTAR code based on radiative hydrodynamic simulations. The results obtained are as follows. (1) The Compton-thin covering factor C_{22} of H I and H II is independent of the Eddington ratio and is approximately 70%, while C_{22} of H I alone is also independent of the Eddington ratio and is approximately 30%. (2) The Compton-thick covering factor C_{24} of H I has the same value as C_{22} of H I. (3) Our C_{24} is consistent with that obtained from X-ray observations. (4) Our C_{22} agrees with that obtained from X-ray observations in a high Eddington ratio, while our C_{22} is smaller than that from X-ray observations in a low Eddington ratio. (5) To explain the difference between C_{22} obtained from theoretical calculations and that inferred from X-ray observations, a Compton-thin gas is required in regions extending at least 10 pc beyond the current computational regions.

Keywords: High energy astrophysics (739), Seyfert galaxies (1447), Supermassive black holes (1663), X-ray active galactic nuclei (2035)

1. INTRODUCTION

The unified model of the active galactic nucleus (AGN) posits that a torus composed of gas and dust exists around an accreting supermassive black hole (SMBH) (R. Antonucci 1993; C. M. Urry & P. Padovani 1995; H. Netzer 2015; C. Ramos Almeida & C. Ricci 2017). The ratio of the solid angle covered by this torus to the SMBH is called the covering factor. Since this covering factor determines the ratio of unobscured to obscured AGNs, estimating its value is crucial. However, the formation mechanisms of the AGN torus and the precise value of the covering factor remain poorly understood.

One of the best tools for estimating the covering factor is X-ray spectroscopic observations. The X-ray spectrum of AGNs consists mainly of two components: a transmitted component absorbed by the torus through photoelectric absorption and a scattered component scattered by the torus through Compton scattering. This allows us to measure the hydrogen column density along the line of sight $N_{\text{H}}^{\text{LOS}}$ based on the shape of the transmitted component (e.g., Y. Ueda et al. 2003, 2014; T. Kawamuro et al. 2016; A. Tanimoto et al. 2016, 2018, 2020; C. Ricci et al. 2017a). In the case of X-ray spectroscopic observations, we classify sources with $N_{\text{H}}^{\text{LOS}}$ smaller than 10^{22} cm^{-2} as unobscured AGNs, those with $N_{\text{H}}^{\text{LOS}}$ between 10^{22} cm^{-2} and 10^{24} cm^{-2} as Compton-thin AGNs, and those with $N_{\text{H}}^{\text{LOS}}$ greater than 10^{24} cm^{-2} as Compton-thick AGNs (e.g., R. C. Hickox & D. M. Alexander 2018). That is, two types of covering factors can be defined. Here we introduce the Compton-thin covering factor C_{22} and the Compton-thick covering factor C_{24} . The Compton-thin covering factor C_{22} is the fraction of the central source covered by gas with $N_{\text{H}}^{\text{LOS}}$ greater

than 10^{22} cm $^{-2}$ and the Compton-thick covering factor C_{24} is the fraction greater than 10^{24} cm $^{-2}$. By measuring the hydrogen column density along the line of sight for a large number of sources, we can statistically determine C_{22} and C_{24} .

C. Ricci et al. (2017a) systematically analyzed the X-ray spectra of 800 AGN detected by the all-sky hard X-ray survey of the Neil Gehrels Swift Observatory (N. Gehrels et al. 2004; C. B. Markwardt et al. 2005; J. Tueller et al. 2010; W. H. Baumgartner et al. 2013; K. Oh et al. 2018) and C. Ricci et al. (2017b) suggested the radiation-regulated AGN unification model. In this model, the Eddington ratio is a key parameter in determining C_{22} . If the Eddington ratio is less than 10^{-2} , C_{22} is a large value of 80%–90%. On the other hand, when the Eddington ratio is greater than 10^{-2} , C_{22} is a small value of 30%–40%. This is because radiation pressure is considered to blow away the dusty gas (C. Ricci et al. 2017b, Figure 4). However, in the X-ray spectral analysis of unobscured AGNs and Compton-thin AGNs, they assumed a simple Compton scattering model (pexrav; P. Magdziarz & A. A. Zdziarski 1995), which is based on flat-plate geometry. This assumption may be inconsistent with their high derived covering factor of 80%–90%.

One of the leading candidates for the AGN torus formation mechanism is the radiation-driven fountain model (K. Wada 2012). In the radiation-driven fountain model, a geometrically thick torus is naturally formed by the anisotropic radiation pressure on the dusty gas and the X-ray heating. In such theoretical calculations, the three-dimensional gas density distribution can be obtained, which allows the covering factor to be calculated directly. The model has successfully reproduced radio (K. Wada et al. 2018a; T. Izumi et al. 2018, 2023; T. Uzuo et al. 2021; S. Baba et al. 2024), infrared (K. Wada et al. 2016; K. Matsumoto et al. 2022, 2023), optical (K. Wada et al. 2018b, 2023), and X-ray observations (S. Ogawa et al. 2022; A. Tanimoto et al. 2023, 2025). These were mainly compared with observations of the Circinus Galaxy, and an Eddington ratio of 20% was assumed.

Y. Kudoh et al. (2024) performed two-dimensional axisymmetric radiative hydrodynamic simulations for four Eddington ratios of 10^{-3} , 10^{-2} , 10^{-1} , and 10^0 with coordinated astronomical numerical software plus (CANS+: Y. Matsumoto et al. 2019). Y. Kudoh et al. (2024) calculated C_{22} for each Eddington ratio based on their radiative hydrodynamic simulations and compared it to the radiation-regulated AGN unification model. As a result, their C_{22} agrees with that inferred from X-ray observations in the low Eddington ratio, whereas their C_{22} is larger than that inferred from X-ray observations in the high Eddington ratio (Y. Kudoh et al. 2024, Figure 9). However, their calculation did not take into account whether hydrogen was H I or H II. Since H II has no electrons, it does not absorb X-rays due to photoelectric absorption. To obtain the covering factor from theoretical calculations and compare it with that obtained from X-ray observations, it is necessary to calculate C_{22} and C_{24} for neutral material.

In this study, to calculate the covering factor of H I, we performed photoionization equilibrium calculations with the XSTAR code (T. R. Kallman et al. 2004) based on two-dimensional axisymmetric radiative hydrodynamic simulations for four Eddington ratios. The remainder of this paper is organized as follows. Section 2 presents the radiative hydrodynamic simulations and the photoionization equilibrium calculations. Section 3 describes the results of the radiative hydrodynamic simulations and the photoionization equilibrium calculations. Section 4 compares the covering factor obtained from our calculations with that inferred from X-ray observations. Finally, Section 5 presents our conclusions.

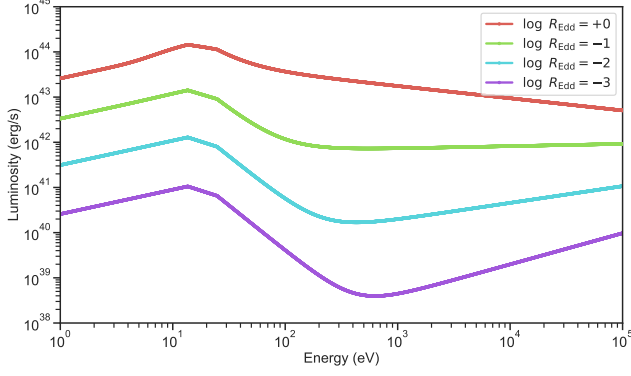


Figure 1. The spectral energy distribution (SED). The red, green, light blue, and purple lines correspond to the SED of the logarithmic Eddington ratio $\log R_{\text{Edd}} = 0, -1, -2$, and -3 , respectively.

2. METHODS

To investigate the H I covering factor, we perform photoionization equilibrium calculations based on two-dimensional axisymmetric radiative hydrodynamic simulations. Section 2.1 describes two-dimensional axisymmetric radiative hydrodynamic simulations and Section 2.2 presents one-dimensional photoionized equilibrium calculations.

2.1. Radiative Hydrodynamic Simulations

Y. Kudoh et al. (2024) performed two-dimensional axisymmetric radiative hydrodynamic simulations of the dusty gas with coordinated astronomical numerical software plus (CANS+: Y. Matsumoto et al. 2019). They solved the following basic equations numerically.

$$\frac{\partial \rho}{\partial t} + \nabla \cdot (\rho \mathbf{v}) = 0 \quad (1)$$

$$\frac{\partial}{\partial t}(\rho \mathbf{v}) + \nabla \cdot (\rho \mathbf{v} \mathbf{v} + P_{\text{gas}} \mathbf{I}) = \mathbf{F}_{\text{grav}} + \mathbf{F}_{\text{radi}} + \mathbf{F}_{\text{vis}} \quad (2)$$

$$\frac{\partial e}{\partial t} + \nabla \cdot (e \mathbf{v} + P_{\text{gas}} \mathbf{v}) = \mathbf{v} \cdot \mathbf{F}_{\text{grav}} + \mathbf{v} \cdot \mathbf{F}_{\text{radi}} + W_{\text{vis}} - \rho \mathcal{L} \quad (3)$$

where ρ is the total density of gas and dust, \mathbf{v} is the velocity, P_{gas} is the gas pressure, \mathbf{F}_{grav} is the gravitational force, \mathbf{F}_{radi} is the radiation force, \mathbf{F}_{vis} is the viscous force, e is the total energy density, W_{vis} is the viscous heating and \mathcal{L} is the heating/cooling rate per unit mass. They assumed that the mass of SMBH was $10^7 M_{\odot}$ and the dust-to-gas ratio is 1%.

They performed two-dimensional axisymmetric radiative hydrodynamic simulations for four different Eddington ratios of $\log R_{\text{Edd}} = -3, -2, -1$, and 0. Figure 1 shows the spectral energy density (SED). The SED is composed of an accretion disk component and a corona component. The component of the accretion disk is based on the Shakura-Sunyaev disk (N. I. Shakura & R. A. Sunyaev 1973; M. Schartmann et al. 2005, 2011) and the component of the corona is assumed to be the power law $L_{\text{corona}}(E) \propto E^{-\Gamma+1}$. In their study, the photon index Γ depends on the Eddington ratio as $\Gamma = 0.32 \log R_{\text{Edd}} + 2.27$ (M. Brightman et al. 2013). The computational domains in the cylindrical coordinate system are $10^{-4} \text{ pc} < r < 2 \text{ pc}$ and $-2 \text{ pc} < z < +2 \text{ pc}$. The boundary condition in the central region of $r \leq 2 \times 10^{-3} \text{ pc}$ is the absorbed boundary conditions with $\rho = 10^{-28} \text{ g cm}^{-3}$ and $T_{\text{gas}} = 10^4 \text{ K}$. The boundary condition in the outer region is the boundary conditions of the outflow.

2.2. Photoionization Equilibrium Calculations

We perform photoionization equilibrium calculations using the XSTAR code (T. R. Kallman et al. 2004) based on two-dimensional axisymmetric radiative hydrodynamic simulations (Y. Kudoh et al. 2024). The XSTAR is a code for calculating the physical conditions and spectra of ionized and nearly neutral gasses. Since XSTAR is a one-zone photoionization equilibrium calculation code, we performed XSTAR calculations for each cell and calculated the photoionization equilibrium from the inside to the outside.

The following five parameters are required to perform XSTAR calculations. (1) inner radius, (2) outer radius, (3) hydrogen number density in the region, (4) shape of the X-ray spectrum and (5) X-ray luminosity at 1–1000 Ry. (1)–(2) We generate a total of 9,000 cells, with the 0.0 pc to 0.1 pc region divided 100 in the radial direction and the 0° to 90° region divided 90 in the angular direction. Although Y. Kudoh et al. (2024) calculated density distributions up to 2 pc (Section 2.1), the inner region has a higher number density. Hence, we performed photoionization equilibrium calculations for the 0.0–0.1 pc region. We confirmed that even when considering up to 2 pc, it does not affect the results obtained. (3) We assumed the hydrogen number density obtained from the radiative hydrodynamic simulations. (4)–(5) In the first cell, the same SED as in the radiative hydrodynamic simulation is assumed. For the second and subsequent cells, the luminosity and spectrum output of the photoionization equilibrium calculations of the previous cell were used. We note that although Y. Kudoh et al. (2024) considered the angular dependence of the disk component, we assumed that the disk component is isotropic. This is because the ionization state is primarily determined by the corona component in our calculations. The solar abundances of E. Anders & N. Grevesse (1989) were assumed.

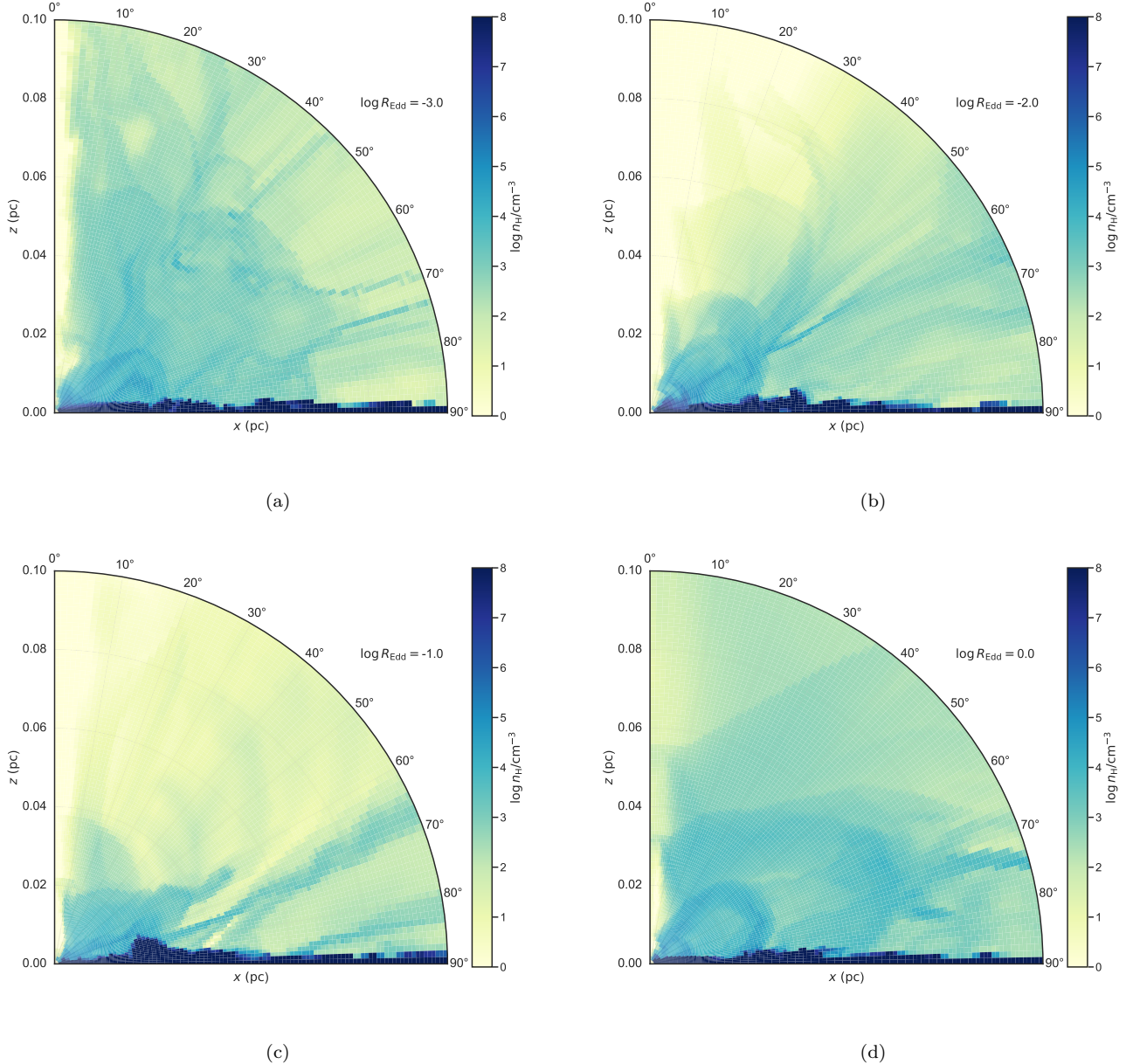


Figure 2. (a) The distribution of the hydrogen number density $\log n_{\text{H}}/\text{cm}^{-3}$ obtained from the radiative hydrodynamic simulation with logarithmic Eddington ratio $\log R_{\text{Edd}}$ of -3 . (b) The $\log n_{\text{H}}/\text{cm}^{-3}$ distribution with $\log R_{\text{Edd}} = -2$. (c) The $\log n_{\text{H}}/\text{cm}^{-3}$ distribution with $\log R_{\text{Edd}} = -1$. (d) The $\log n_{\text{H}}/\text{cm}^{-3}$ distribution with $\log R_{\text{Edd}} = 0$.

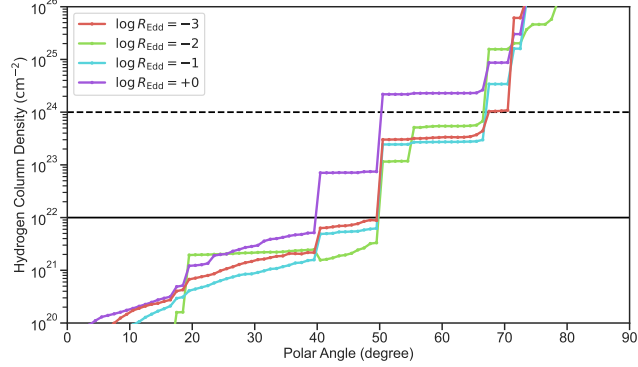


Figure 3. The averaged hydrogen column density as a function of the polar angle. The red, green, light blue, and purple lines correspond to the radiative hydrodynamic simulations of $\log R_{\text{Edd}} = -3, -2, -1$, and 0 , respectively. The solid, and dashed lines represent the hydrogen column density of 10^{22} cm^{-2} and 10^{24} cm^{-2} , respectively.

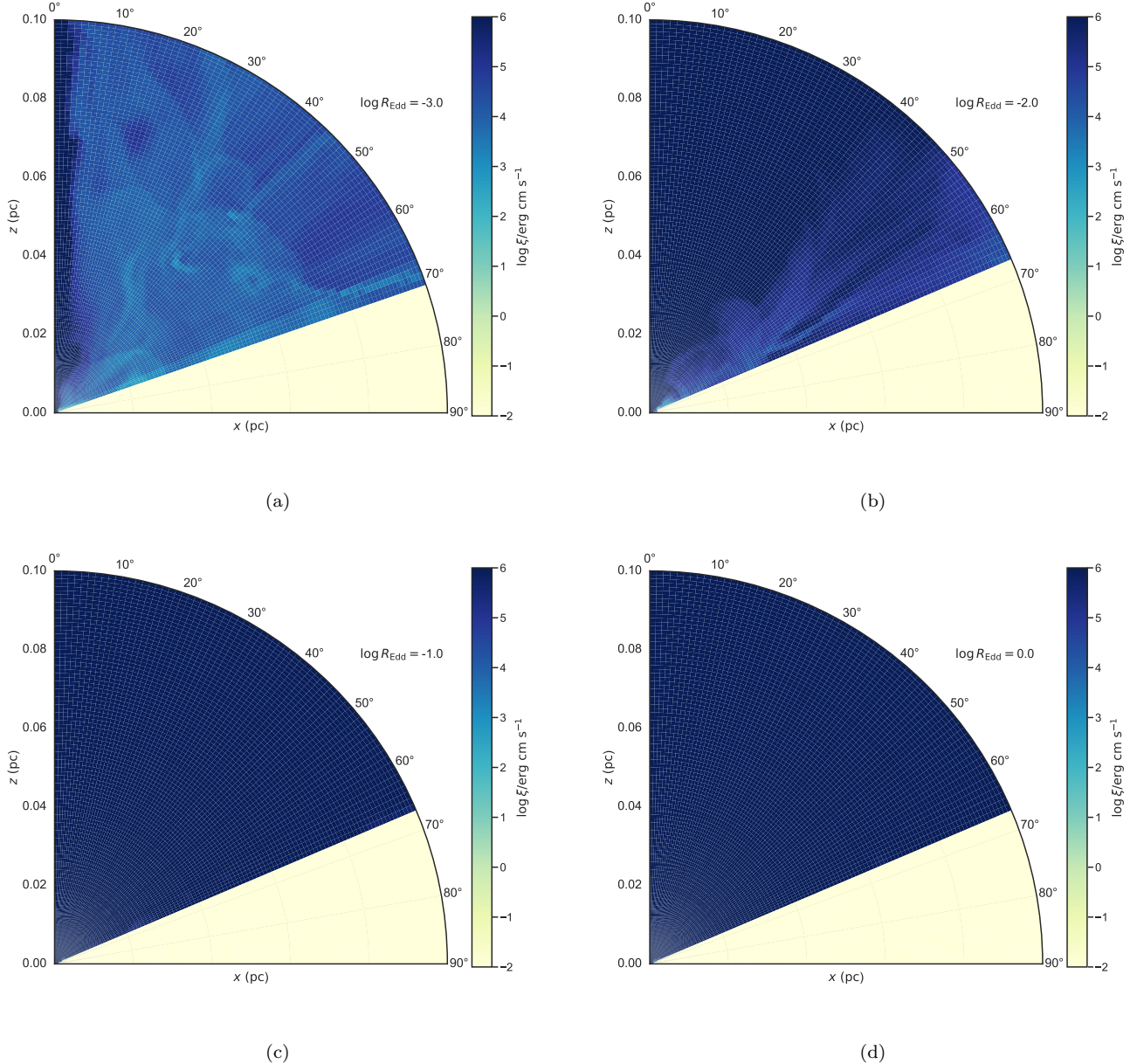


Figure 4. (a) The distribution of the ionization parameter $\log \xi/\text{erg cm s}^{-1}$ obtained from the radiative hydrodynamic simulation with logarithmic Eddington ratio $\log R_{\text{Edd}}$ of -3 . (b) The $\log \xi/\text{erg cm s}^{-1}$ distribution with $\log R_{\text{Edd}} = -2$. (c) The $\log \xi/\text{erg cm s}^{-1}$ distribution with $\log R_{\text{Edd}} = -1$. (d) The $\log \xi/\text{erg cm s}^{-1}$ distribution with $\log R_{\text{Edd}} = 0$.

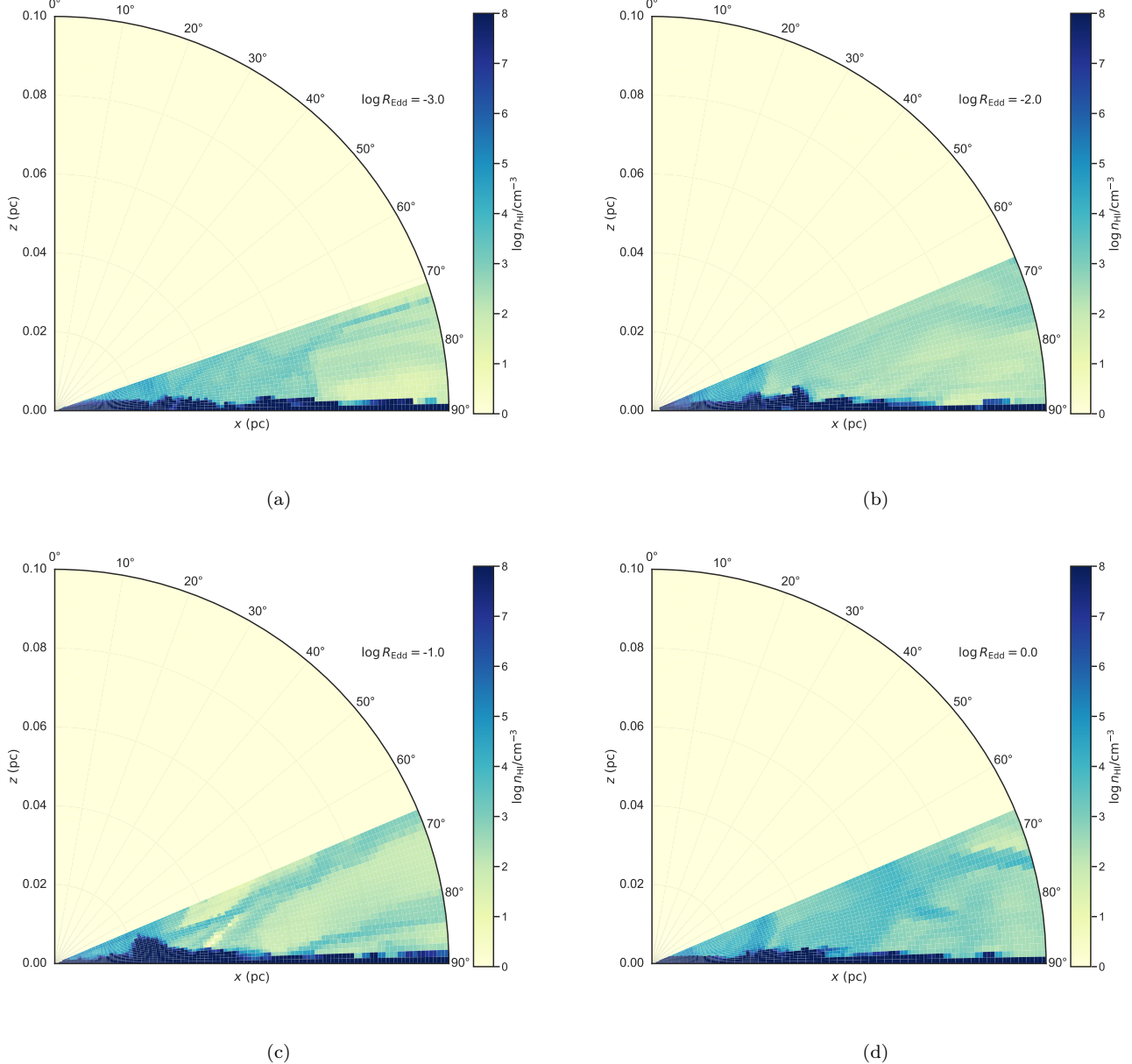


Figure 5. (a) The distribution of H I number density $\log n_{\text{HI}}/\text{cm}^{-3}$ obtained from the radiative hydrodynamic simulation with logarithmic Eddington ratio $\log R_{\text{Edd}}$ of -3 . (b) The $\log n_{\text{HI}}/\text{cm}^{-3}$ distribution with $\log R_{\text{Edd}} = -2$. (c) The $\log n_{\text{HI}}/\text{cm}^{-3}$ distribution with $\log R_{\text{Edd}} = -1$. (d) The $\log n_{\text{HI}}/\text{cm}^{-3}$ distribution with $\log R_{\text{Edd}} = 0$.

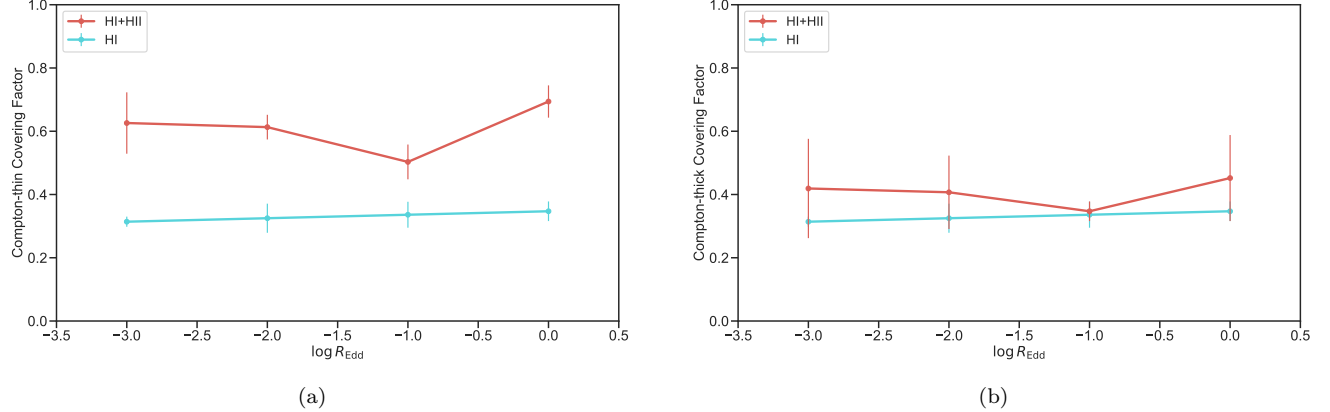


Figure 6. (a) The relationship between the Eddington ratio and the Compton-thin covering factor C_{22} . The red line represents H I and H II C_{22} . The light blue line corresponds to H I C_{22} . (b) The relationship between the Eddington ratio and the Compton-thick covering factor C_{24} . The red line represents H I and H II C_{24} . The light blue line corresponds to H I C_{24} .

3. RESULTS

[Section 3.1](#) presents the dependence of the hydrogen number density distribution on the Eddington ratio. [Section 3.2](#) shows the dependence of the distribution of the ionization parameter on the Eddington ratio. [Section 3.3](#) presents the dependence of the H I number density distribution on the Eddington ratio. [Section 3.4](#) shows the H I Compton-thin covering factor and the H I Compton-thick covering factor as a function of the Eddington ratio.

3.1. *Dependence of Hydrogen Number Density Distribution on Eddington Ratio*

We studied the dependence of the hydrogen number density $\log n_{\text{H}}/\text{cm}^{-3}$ distribution on the Eddington ratio. [Figure 2](#) show $\log n_{\text{H}}/\text{cm}^{-3}$ distributions obtained from radiative hydrodynamic simulations with (a) the logarithmic Eddington ratio $\log R_{\text{Edd}} = -3$, (b) $\log R_{\text{Edd}} = -2$, (c) $\log R_{\text{Edd}} = -1$, and (d) $\log R_{\text{Edd}} = 0$. All density distributions consist of dense material in the equatorial plane with $\log n_{\text{H}}/\text{cm}^{-3} \simeq 8$ and outflow with $\log n_{\text{H}}/\text{cm}^{-3} \simeq 4$.

The physical quantity obtained from the observation is not the hydrogen number density, but the hydrogen column density. The hydrogen number density distribution obtained from simulations evolves over time. To investigate the averaged hydrogen column density, we averaged the hydrogen number density distributions obtained from snapshots at $t = 0, 30, 60$, and 90 years. [Figure 3](#) shows the averaged hydrogen column density as a function of the polar angle θ . In the case of $\log R_{\text{Edd}} = -3, -2$, and -1 , the hydrogen column density reaches 10^{22} cm^{-2} at $\theta = 50^\circ$. In the case of $\log R_{\text{Edd}} = 0$, the hydrogen column density reaches 10^{22} cm^{-2} at $\theta = 40^\circ$. That is, the relationship between the polar angle and the hydrogen column density does not change significantly even as the Eddington ratio increases. If the hydrogen column density along the line of sight exceeds 10^{25} cm^{-2} , even X-rays cannot penetrate it. Since all models have hydrogen column densities exceeding 10^{25} cm^{-2} at polar angle between 65° and 75° , regions with polar angle greater than these values are expected to be almost neutral.

3.2. *Dependence of Ionization Parameter Distribution on the Eddington Ratio*

We perform one-dimensional photoionization equilibrium calculations based on radiative hydrodynamic simulations. [Figure 4](#) shows the distributions of the ionization parameters $\log \xi/\text{erg cm s}^{-1}$ with (a) $\log R_{\text{Edd}} = -3$, (b) $\log R_{\text{Edd}} = -2$, (c) $\log R_{\text{Edd}} = -1$, and (d) $\log R_{\text{Edd}} = 0$. Here, the ionization parameter ξ is defined as $\xi = L/n_{\text{H}}r^2$, where L is the luminosity in 1–1000 Ryd, n_{H} is the hydrogen number density, and r is the distance from the central source.

[Figure 4](#) indicates that the distribution of $\log \xi/\text{erg cm s}^{-1}$ varies greatly between θ of 65° and 75° . If θ is less than 70° , the ionization parameters are proportional to the luminosity of the central source because the line of sight is optically thin. In particular, for models with a low Eddington ratio, this region exhibits a moderate ionization parameter with $\log \xi/\text{erg cm s}^{-1} = 2–4$, which makes it likely to be observed as warm absorbers. Since we plan to perform three-dimensional X-ray radiative transfer calculations based on these models in future papers, we will not address warm absorbers in this paper. When θ is greater than 70° , the ionization parameters are independent of the Eddington ratio and are nearly neutral. This is because, as explained in [Section 3.1](#), the line of sight is optically thick and the X-rays are almost completely absorbed.

3.3. Dependence of Neutral Hydrogen Number Density Distribution on the Eddington Ratio

To calculate the covering factor for the neutral material, the distribution of H I number density is required. Since we obtain H I and H II fractions for each region from XSTAR calculations, we define the H I number density in each region as the hydrogen number density multiplied by the H I fraction. Figure 5 shows the distribution of the H I number density $\log n_{\text{HI}}/\text{cm}^{-3}$ with (a) $\log R_{\text{Edd}} = -3$, (b) $\log R_{\text{Edd}} = -2$, (c) $\log R_{\text{Edd}} = -1$, and (d) $\log R_{\text{Edd}} = 0$. Figure 5 shows only the region in Figure 2 where the logarithmic ionization parameter is less than -2 . The reason is that, for H I to exist, the logarithmic ionization parameter must be less than -2 (T. R. Kallman & R. McCray 1982, Figure 1). As explained in Section 3.2, the region where θ is greater than 70° is nearly neutral (Figure 4). Figure 5 indicates that H I can survive only in the region where θ is greater than 70° .

We note that even if all H I becomes H II, it does not mean that the material around the AGN will not absorb X-rays through photoelectric absorption. This is because the material around AGNs not only contains hydrogen but also helium, carbon, oxygen, neon, magnesium, silicon, sulfur, iron, nickel, and others. When estimating the hydrogen column density along the line of sight from X-ray spectroscopic observations, the X-ray spectrum in the 2–8 keV energy band is frequently utilized. In this energy band, photoelectric absorption by O I is the primary process (R. Morrison & D. McCammon 1983; B. Vander Meulen et al. 2023). When the logarithmic ionization parameter is greater than 2, since almost all oxygen becomes O IX, X-ray absorption due to photoelectric absorption becomes very weak (T. R. Kallman & R. McCray 1982, Figure 1). This does not affect the results of this paper. The reason is that the logarithmic ionization parameter has discrete values of -2 and $+2$ around $\theta = 70^\circ$ (Figure 4).

3.4. Covering Factor of Neutral Hydrogen

We calculated the H I covering factor based on radiative hydrodynamic simulations and photoionization equilibrium calculations. Figure 6(a) compares C_{22} of H I alone with C_{22} of H I and H II. Since the density structures in the simulations vary over time, we obtain the covering factor averaged in time from four snapshots at $t = 0, 30, 60$, and 90 years. Here, the error corresponds to 1σ . The Compton-thin covering factors C_{22} of H I and H II are almost independent of the Eddington ratio and are approximately 70%. The Compton-thin covering factors C_{22} of H I alone are also independent of the Eddington ratio and are approximately 30%. Since the region within 0.1 pc is photoionized even in an Eddington ratio of 10^{-3} , C_{22} of H I is independent of the Eddington ratio. Figure 6(b) compares C_{24} of H I alone with C_{24} of H I and H II. The Compton-thick covering factors C_{24} of H I and H II are smaller than C_{22} and are approximately 40%. The Compton-thick covering factors C_{24} of H I alone are independent of the Eddington ratio and are approximately 30%. In the case of the region under consideration, since all Compton-thin gasses are photoionized, H I C_{24} has the same value as H I C_{22} .

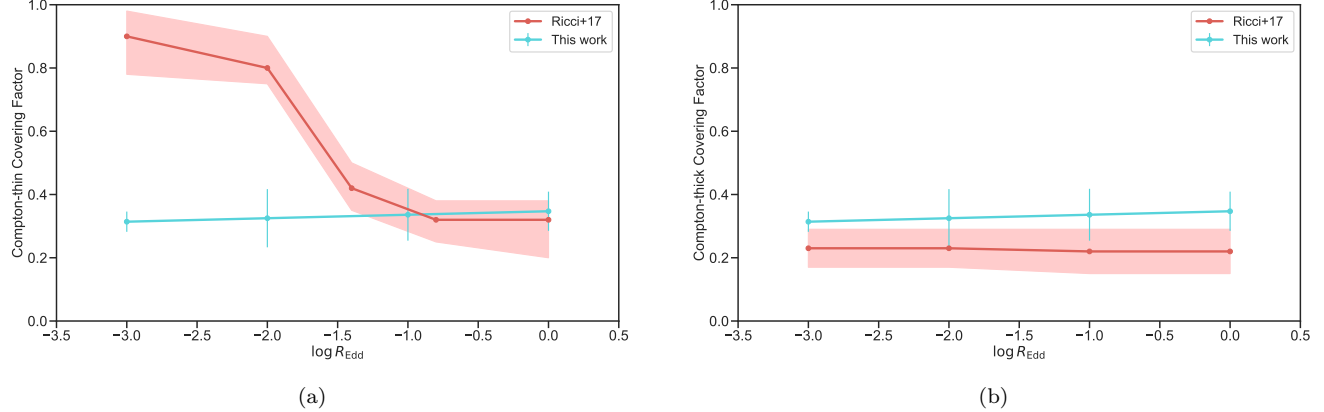


Figure 7. (a) The comparison between the Compton-thin covering factor C_{22} obtained from our simulation and that inferred from X-ray observations. The red line represents C_{22} obtained from the X-ray observations (C. Ricci et al. 2017b). The light blue line corresponds to C_{22} obtained from our simulation. (b) The comparison between the Compton-thick covering factor C_{24} obtained from our simulation and that inferred from the X-ray observations. The red line represents C_{24} obtained from the X-ray observations. The light blue line corresponds to C_{24} obtained from our simulation.

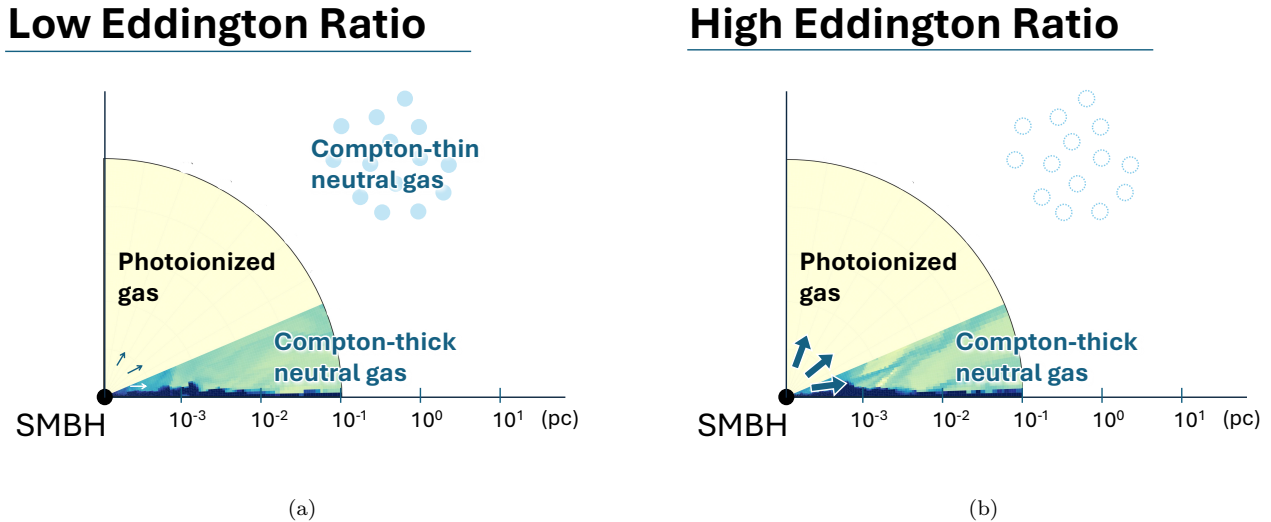


Figure 8. Schematic diagram of a unified model of AGN based on photoionization equilibrium. In both cases, Compton-thick neutral gas with a covering factor of approximately 30% exists at a distance of approximately 10^{-3} – 10^{-1} pc. If the Eddington ratio is less than 10^{-2} , Compton-thin neutral gas exists at a distance of approximately 10 pc. When the Eddington ratio is greater than 10^{-1} , since the Compton-thin neutral gas is photoionized, the covering factor of the Compton-thin gas decreases.

4. DISCUSSION

To estimate the covering factor of H I, we performed photoionization equilibrium calculations based on radiative hydrodynamic simulations. Section 4.1 compares the covering factor obtained from our simulation with that inferred from the X-ray observations. Section 4.2 discusses the physical mechanisms that determine the covering factor. Section 4.3 proposes an AGN unified model based on photoionization.

4.1. Comparison of Covering Factors

We compare the covering factor obtained from theoretical calculations with that inferred from X-ray observations. Figure 7(b) compares the results of C_{24} obtained from our simulations with that inferred from the X-ray observations (C. Ricci et al. 2017b). As explained in Section 3.4, our C_{24} is independent of the Eddington ratio and is approximately 30%. Our C_{24} is consistent with that obtained from the X-ray observations (C. Ricci et al. 2017b; A. Tanimoto et al. 2022; P. G. Boorman et al. 2025). In other words, our model, which considers the region from 10^{-3} to 10^{-1} pc, can explain C_{24} obtained from X-ray observations.

Figure 7(a) compares the results of C_{22} obtained from our simulations with that inferred from the X-ray observations. Our C_{22} is independent of the Eddington ratio and is approximately 30%. When the Eddington ratio is greater than 10^{-1} , our C_{22} is consistent with that obtained from the X-ray observations. If the Eddington ratio is smaller than 10^{-2} , our C_{22} is smaller than that obtained from the X-ray observations. This is because even if Compton-thin gas exists inside 0.1 pc, it is photoionized by X-ray radiation from the central source.

4.2. Physical Mechanism Determining Covering Factor

The radiation-regulated AGN unification model considers that the radiation pressure blows off a Compton-thin dusty gas when the Eddington ratio is greater than 10^{-2} . Although AGNs radiation plays a significant role as the physical mechanism that determines the covering factor, it remains unclear whether the primary effect is the radiation pressure blowing away matter or the photoionization of matter by radiation.

To distinguish them, we investigated the dependence of the hydrogen column density on the polar angle. We can directly examine the relationship between the polar angle and the hydrogen column density based on radiative hydrodynamic simulations. As shown in Figure 3, the relationship between the polar angle and the hydrogen column density does not change significantly even when the Eddington ratio changes inside 0.1 pc. Our result is consistent with Y. Kudoh et al. (2024). Y. Kudoh et al. (2024) showed the hydrogen column densities as a function of the elevation angle for dusty and dust-free gasses. They suggested that the hydrogen column density of dusty gas decreases with the Eddington ratio, whereas that of dust-free gas is nearly independent of the Eddington ratio.

In their calculations, the hydrogen column density is primarily determined by hot, dust-free ionized gas located inside the dust sublimation radius. Since dusty gas located outside the sublimation radius is efficiently accelerated and expanded due to radiation pressure on the dust, their hydrogen column densities are not large. In contrast, the dust-free gas experiences weaker radiative acceleration and tends to remain gravitationally bound, maintaining relatively high number density (Y. Kudoh et al. 2023, Figure 6). Hence, the hydrogen column density is dominated by dust-free gas rather than dust gas and is almost independent of the Eddington ratio (Y. Kudoh et al. 2024, Figure 8). This is consistent with the observations of the nearby AGN (L. Burtscher et al. 2016; S. Mizukoshi et al. 2024). S. Mizukoshi et al. (2024) indicated that the hydrogen column density of dust-free gas is basically greater than that of dusty gas (S. Mizukoshi et al. 2024, Figure 4). That is, within the region less than 0.1 pc, the effect of photoionization is more significant than the effect of blowing away matter through radiation pressure.

4.3. AGN Unified Model via Photoionization

Since our C_{22} has the same value as our C_{24} , all AGNs are observed to be unobscured or Compton-thick AGNs. However, X-ray observations reveal that many Compton-thin AGNs are present (e.g., T. Kawamuro et al. 2016). To explain the existence of these Compton-thin AGNs, H I must be present in regions beyond the current computational domain. If the Eddington ratio is 10^{-2} , we can estimate the lower limit of the distance to the absorber under the condition that the Compton-thin H I survives

$$\begin{cases} 10^{22} \text{ cm}^{-2} \leq N_{\text{H}} & < 10^{24} \text{ cm}^{-2} \\ \frac{L(R_{\text{Edd}}=10^{-2})}{n_{\text{H}} r^2} & \leq 10^{-2} \text{ erg cm s}^{-1} \end{cases} \quad (4)$$

Here, N_{H} is the hydrogen column density along the line of sight, $L(R_{\text{Edd}} = 10^{-2})$ is the X-ray luminosity at the Eddington ratio of 10^{-2} , n_{H} is the hydrogen number density, and r is the distance to the absorber. We assume that the hydrogen column density is expressed as $N_{\text{H}} = n_{\text{H}} r f$, where f is the filling factor. Substituting the first equation of Equation 4 into the second equation of Equation 4 and simplifying produces the following lower limit for the distance to the absorber.

$$r \geq 30 \left(\frac{N_{\text{H}}}{10^{22} \text{ cm}^{-2}} \right)^{-1} \left(\frac{L}{10^{42} \text{ erg s}^{-1}} \right) \left(\frac{f}{10^{-2}} \right) \text{ pc.} \quad (5)$$

If the hydrogen column density is 10^{22} cm^{-2} , the X-ray luminosity is $10^{42} \text{ erg s}^{-1}$, and the filling factor is 10^{-2} , the Compton-thin gas must exist beyond 30 pc. This radius extends beyond the computational domain of the current radiative hydrodynamic simulations. If a Compton-thin gas exists at this radius, it could explain the discrepancy between C_{22} obtained from theoretical calculations and those derived from X-ray observations.

Figure 8 shows a schematic diagram of the unified model of AGN based on photoionization equilibrium. A Compton-thick neutral gas with a covering factor of approximately 30% exists at a distance of approximately 10^{-3} – 10^{-1} pc. If the Eddington ratio is smaller than 10^{-2} , a Compton-thin neutral gas exists at a distance of approximately 30 pc. When the Eddington ratio is greater than 10^{-1} , since the Compton-thin gas is photoionized, the covering factor becomes smaller. Note that the physical mechanism to blow off the Compton-thin gas to a large-scale height is an open question.

5. CONCLUSION

To clarify the relationship between the Eddington ratio and the covering factor, we performed the photoionization equilibrium calculations based on the two-dimensional axisymmetric radiative hydrodynamic simulations for four Eddington ratios. We calculated the Compton-thin covering factor C_{22} and Compton-thick covering factor C_{24} and compared those obtained from theoretical calculations with those inferred from X-ray observations. The key findings are as follows.

1. H I and H II C_{22} is independent of the Eddington ratio and is approximately 70%. H I C_{22} is also independent of the Eddington ratio and is approximately 30%. This is because the Compton-thin gas within 0.1 pc is photoionized by the radiation from the central source even at an Eddington ratio of 10^{-3} .
2. We compared C_{24} obtained from our simulation with that inferred from X-ray observations. Our C_{24} is consistent with that inferred from the X-ray observations. This result suggests that the Compton-thick gases are formed by a radiation-driven fountain model.
3. Our C_{22} agrees with that inferred from X-ray observations in a high Eddington ratio, whereas our C_{22} is smaller than that from X-ray observations in a low Eddington ratio. To account for the large C_{22} obtained from X-ray observations, a Compton-thin gas with a radius of approximately 10 pc is required.
4. The relationship between the hydrogen column density and the polar angle is found to be almost independent of the Eddington ratio. This suggests that the covering factor is mainly determined by photoionization within the region inside 0.1 pc.

ACKNOWLEDGEMENTS

The authors thank the anonymous referee who provided useful and detailed comments. Atsushi Tanimoto and the present research are supported by the Kagoshima University postdoctoral research program (KU-DREAM). This work is also supported by the Grant-in-Aid for Early Career Scientists Grant No. 23K13147 (A.T.), the Grants-in-Aid for Scientific Research Grant Nos. 25H00671 (K.W.), 24K17080 (Y.K.), and 22H00128 (H.O.), and the Exploratory Research Grant for Young Scientists, Hirosaki University (M.N.). Numerical computations were performed on Cray XD2000 at the Center for Computational Astrophysics, National Astronomical Observatory of Japan.

Software: XSTAR ([T. R. Kallman et al. 2004](#))

REFERENCES

- Anders, E., & Grevesse, N. 1989, *GeoCoA*, 53, 197, doi: [10.1016/0016-7037\(89\)90286-X](https://doi.org/10.1016/0016-7037(89)90286-X)
- Antonucci, R. 1993, *ARA&A*, 31, 473, doi: [10.1146/annurev.aa.31.090193.002353](https://doi.org/10.1146/annurev.aa.31.090193.002353)
- Baba, S., Wada, K., Izumi, T., Kudoh, Y., & Matsumoto, K. 2024, *ApJ*, 966, 15, doi: [10.3847/1538-4357/ad34d3](https://doi.org/10.3847/1538-4357/ad34d3)
- Baumgartner, W. H., Tueller, J., Markwardt, C. B., et al. 2013, *ApJS*, 207, 19, doi: [10.1088/0067-0049/207/2/19](https://doi.org/10.1088/0067-0049/207/2/19)
- Boorman, P. G., Gandhi, P., Buchner, J., et al. 2025, *ApJ*, 978, 118, doi: [10.3847/1538-4357/ad8236](https://doi.org/10.3847/1538-4357/ad8236)
- Brightman, M., Silverman, J. D., Mainieri, V., et al. 2013, *MNRAS*, 433, 2485, doi: [10.1093/mnras/stt920](https://doi.org/10.1093/mnras/stt920)
- Burtscher, L., Davies, R. I., Graciá-Carpio, J., et al. 2016, *A&A*, 586, A28, doi: [10.1051/0004-6361/201527575](https://doi.org/10.1051/0004-6361/201527575)
- Gehrels, N., Chincarini, G., Giommi, P., et al. 2004, *ApJ*, 611, 1005, doi: [10.1086/422091](https://doi.org/10.1086/422091)
- Hickox, R. C., & Alexander, D. M. 2018, *ARA&A*, 56, 625, doi: [10.1146/annurev-astro-081817-051803](https://doi.org/10.1146/annurev-astro-081817-051803)
- Izumi, T., Wada, K., Fukushige, R., Hamamura, S., & Kohno, K. 2018, *ApJ*, 867, 48, doi: [10.3847/1538-4357/aae20b](https://doi.org/10.3847/1538-4357/aae20b)
- Izumi, T., Wada, K., Imanishi, M., et al. 2023, *Science*, 382, 554, doi: [10.1126/science.adf0569](https://doi.org/10.1126/science.adf0569)
- Kallman, T. R., & McCray, R. 1982, *ApJS*, 50, 263, doi: [10.1086/190828](https://doi.org/10.1086/190828)
- Kallman, T. R., Palmeri, P., Bautista, M. A., Mendoza, C., & Krolik, J. H. 2004, *ApJS*, 155, 675, doi: [10.1086/424039](https://doi.org/10.1086/424039)
- Kawamuro, T., Ueda, Y., Tazaki, F., Ricci, C., & Terashima, Y. 2016, *ApJS*, 225, 14, doi: [10.3847/0067-0049/225/1/14](https://doi.org/10.3847/0067-0049/225/1/14)
- Kudoh, Y., Wada, K., Kawakatu, N., & Nomura, M. 2023, *ApJ*, 950, 72, doi: [10.3847/1538-4357/accc2b](https://doi.org/10.3847/1538-4357/accc2b)
- Kudoh, Y., Wada, K., Kawakatu, N., & Nomura, M. 2024, *ApJ*, 977, 48, doi: [10.3847/1538-4357/ad8b42](https://doi.org/10.3847/1538-4357/ad8b42)
- Magdziarz, P., & Zdziarski, A. A. 1995, *MNRAS*, 273, 837, doi: [10.1093/mnras/273.3.837](https://doi.org/10.1093/mnras/273.3.837)
- Markwardt, C. B., Tueller, J., Skinner, G. K., et al. 2005, *ApJL*, 633, L77, doi: [10.1086/498569](https://doi.org/10.1086/498569)
- Matsumoto, K., Camps, P., Baes, M., et al. 2023, *A&A*, 678, A175, doi: [10.1051/0004-6361/202347376](https://doi.org/10.1051/0004-6361/202347376)
- Matsumoto, K., Nakagawa, T., Wada, K., et al. 2022, *ApJ*, 934, 25, doi: [10.3847/1538-4357/ac755f](https://doi.org/10.3847/1538-4357/ac755f)
- Matsumoto, Y., Asahina, Y., Kudoh, Y., et al. 2019, *PASJ*, 71, 83, doi: [10.1093/pasj/psz064](https://doi.org/10.1093/pasj/psz064)
- Mizukoshi, S., Minezaki, T., Sameshima, H., et al. 2024, *MNRAS*, 532, 666, doi: [10.1093/mnras/stae1482](https://doi.org/10.1093/mnras/stae1482)
- Morrison, R., & McCammon, D. 1983, *ApJ*, 270, 119, doi: [10.1086/161102](https://doi.org/10.1086/161102)
- Netzer, H. 2015, *ARA&A*, 53, 365, doi: [10.1146/annurev-astro-082214-122302](https://doi.org/10.1146/annurev-astro-082214-122302)
- Ogawa, S., Ueda, Y., Wada, K., & Mizumoto, M. 2022, *ApJ*, 925, 55, doi: [10.3847/1538-4357/ac3cb9](https://doi.org/10.3847/1538-4357/ac3cb9)
- Oh, K., Koss, M., Markwardt, C. B., et al. 2018, *ApJS*, 235, 4, doi: [10.3847/1538-4365/aaa7fd](https://doi.org/10.3847/1538-4365/aaa7fd)
- Ramos Almeida, C., & Ricci, C. 2017, *Nature Astronomy*, 1, 679, doi: [10.1038/s41550-017-0232-z](https://doi.org/10.1038/s41550-017-0232-z)
- Ricci, C., Trakhtenbrot, B., Koss, M. J., et al. 2017a, *ApJS*, 233, 17, doi: [10.3847/1538-4365/aa96ad](https://doi.org/10.3847/1538-4365/aa96ad)
- Ricci, C., Trakhtenbrot, B., Koss, M. J., et al. 2017b, *Nature*, 549, 488, doi: [10.1038/nature23906](https://doi.org/10.1038/nature23906)
- Schartmann, M., Krause, M., & Burkert, A. 2011, *MNRAS*, 415, 741, doi: [10.1111/j.1365-2966.2011.18751.x](https://doi.org/10.1111/j.1365-2966.2011.18751.x)
- Schartmann, M., Meisenheimer, K., Camenzind, M., Wolf, S., & Henning, T. 2005, *A&A*, 437, 861, doi: [10.1051/0004-6361:20042363](https://doi.org/10.1051/0004-6361:20042363)
- Shakura, N. I., & Sunyaev, R. A. 1973, *A&A*, 24, 337
- Tanimoto, A., Ueda, Y., Kawamuro, T., & Ricci, C. 2016, *PASJ*, 68, S26, doi: [10.1093/pasj/psw008](https://doi.org/10.1093/pasj/psw008)
- Tanimoto, A., Ueda, Y., Kawamuro, T., et al. 2018, *ApJ*, 853, 146, doi: [10.3847/1538-4357/aaa47c](https://doi.org/10.3847/1538-4357/aaa47c)
- Tanimoto, A., Ueda, Y., Odaka, H., et al. 2020, *ApJ*, 897, 2, doi: [10.3847/1538-4357/ab96bc](https://doi.org/10.3847/1538-4357/ab96bc)
- Tanimoto, A., Ueda, Y., Odaka, H., Yamada, S., & Ricci, C. 2022, *ApJS*, 260, 30, doi: [10.3847/1538-4365/ac5f59](https://doi.org/10.3847/1538-4365/ac5f59)
- Tanimoto, A., Wada, K., Kudoh, Y., et al. 2023, *ApJ*, 958, 150, doi: [10.3847/1538-4357/ad06ac](https://doi.org/10.3847/1538-4357/ad06ac)
- Tanimoto, A., Wada, K., Odaka, H., Kudoh, Y., & Nozomu, K. 2025, arXiv e-prints, arXiv:2505.09693, doi: [10.48550/arXiv.2505.09693](https://doi.org/10.48550/arXiv.2505.09693)
- Tueller, J., Baumgartner, W. H., Markwardt, C. B., et al. 2010, *ApJS*, 186, 378, doi: [10.1088/0067-0049/186/2/378](https://doi.org/10.1088/0067-0049/186/2/378)
- Ueda, Y., Akiyama, M., Hasinger, G., Miyaji, T., & Watson, M. G. 2014, *ApJ*, 786, 104, doi: [10.1088/0004-637X/786/2/104](https://doi.org/10.1088/0004-637X/786/2/104)
- Ueda, Y., Akiyama, M., Ohta, K., & Miyaji, T. 2003, *ApJ*, 598, 886, doi: [10.1086/378940](https://doi.org/10.1086/378940)
- Urry, C. M., & Padovani, P. 1995, *PASP*, 107, 803, doi: [10.1086/133630](https://doi.org/10.1086/133630)
- Uzuo, T., Wada, K., Izumi, T., et al. 2021, *ApJ*, 915, 89, doi: [10.3847/1538-4357/ac013d](https://doi.org/10.3847/1538-4357/ac013d)
- Vander Meulen, B., Camps, P., Stalevski, M., & Baes, M. 2023, *A&A*, 674, A123, doi: [10.1051/0004-6361/202245783](https://doi.org/10.1051/0004-6361/202245783)
- Wada, K. 2012, *ApJ*, 758, 66, doi: [10.1088/0004-637X/758/1/66](https://doi.org/10.1088/0004-637X/758/1/66)
- Wada, K., Fukushige, R., Izumi, T., & Tomisaka, K. 2018a, *ApJ*, 852, 88, doi: [10.3847/1538-4357/aa9e53](https://doi.org/10.3847/1538-4357/aa9e53)

Wada, K., Kudoh, Y., & Nagao, T. 2023, MNRAS, 526, 2717, doi: [10.1093/mnras/stad2918](https://doi.org/10.1093/mnras/stad2918)

Wada, K., Schartmann, M., & Meijerink, R. 2016, ApJL, 828, L19, doi: [10.3847/2041-8205/828/2/L19](https://doi.org/10.3847/2041-8205/828/2/L19)

Wada, K., Yonekura, K., & Nagao, T. 2018b, ApJ, 867, 49, doi: [10.3847/1538-4357/aae204](https://doi.org/10.3847/1538-4357/aae204)